Journal of Peptide Science
J. Peptide Sci. **5**: 491–506 (1999)

Conformations and Pharmacophores of Cyclic RGD Containing Peptides which Selectively Bind Integrin $\alpha_v\beta_3$

ELSA LOCARDI[a], DANIEL G. MULLEN[b], RALPH-HEIKO MATTERN[b] and MURRAY GOODMAN[b,*]

[a] Department of Chemistry and Biochemistry, University of California, San Diego, USA
[b] Integra LifeSciences Corporation, Corporate Research Center. San Diego, CA 92121, USA

Received 19 April 1999
Accepted 20 May 1999

Abstract: This paper reports a detailed conformational characterization in solution by ^{1}H-NMR in H_2O and DMSO-d_6 and molecular modeling simulations of cyclic peptides containing the RGDDV pharmacophore and the RGDY(Me)R pharmacophore. These two pentapeptide sequences when properly constrained in cyclic peptides are low to sub-nanomolar inhibitors of integrin $\alpha_v\beta_3$. The peptides containing the RGDDY(Me)R sequence bind potently to integrin $\alpha_{IIb}\beta_3$ as well. The conformations found in H_2O and in DMSO-d_6 solutions are valuable for the design of peptidomimetics of these two pharmacophores. The structure–activity relationships of the RGDDV and RGDY(Me)R pharmacophores within cyclic peptides are discussed. Specifically, the orientation of surface-accessible chemical features on the ligand, such as hydrophobic, positive and negative ionizable groups, which are considered to be responsible for the desired biological activity, is focused on. Copyright © 1999 European Peptide Society and John Wiley & Sons, Ltd.

Keywords: RGD; integrins $\alpha_v\beta_3$ and $\alpha_{IIb}\beta_3$; molecular dynamics; nuclear magnetic resonance; peptide conformations

INTRODUCTION

Integrins are heterodimeric cell surface receptors that mediate cell-cell and cell-extracellular matrix interactions. A subset of integrins bind the RGD tripeptide sequence which is found in numerous extracellular matrix proteins such as fibronectin, vitronectin, and fibrinogen [1]. Antagonists to integrin $\alpha_v\beta_3$, a vitronectin receptor, may be useful as therapeutics in a number of areas including metastasis, osteoporosis, and the inhibition of angiogenesis [2–4].

A number of research groups have reported potent peptide and peptidomimetic antagonists to the $\alpha_v\beta_3$ receptor [5–10]. Two pentapeptide pharmacophores have been discovered that exhibit unique activity/selectivity profiles at this receptor. The first pharmacophore, the RGDDV sequence, binds integrin $\alpha_v\beta_3$ with 100–1000-fold selectivity as compared to integrins $\alpha_v\beta_5$, $\alpha_{IIb}\beta_3$, $\alpha_5\beta_1$ [11]. The second pharmacophore, the RGDDY(Me)R sequence, was developed as a platelet glycoprotein IIb/IIIa ($\alpha_{IIb}\beta_3$) antagonist [12–14]. Subsequently, the sequence has been found to selectively bind integrins which contain the β_3 receptor [15,16].

Table 1 shows the binding activity of selected peptides to various integrin receptors. The sequences of the six cyclic peptides chosen for conformational analysis are reported in Scheme 1. The linear peptide **7** which contains the RGDDV pharmacophore, exhibits low affinity for the $\alpha_v\beta_3$ receptor. Constraining the sequence through disulfide cyclization between 3-mercaptopropionic acid (Mpa) and cysteine increases the activity $\approx$70-fold (c[MpaRGDDVC]-NH_2, **8**). Replacement of valine with the more hydrophobic and highly β-branched amino acid L-*tert*-butylglycine (*t*-BuG) gives rise to a slight increase in activity (**4**). Further constraining the sequence by *N*- to *C*-terminal cyclization with *m*-(aminomethyl)benzoic acid (Mamb) (**1**) produces another 10-fold increase in potency. Compound **1** is

* Correspondence to: Department of Chemistry and Biochemistry University of California at San Diego, La Jolla, CA 92093-0343, USA.

CCC 1075–2617/99/110491-16$17.50

≈2700 times more active than linear **7** in inhibiting vitronectin binding to $\alpha_v\beta_3$. It is noteworthy that compound **1** is also expected to be the least flexible in solution due to the incorporation of the planar aromatic system of the Mamb moiety. This residue contains only three freely rotating bonds as compared to seven in the disulfide linkage of compound **4** (Scheme 2). Replacing Mamb with the longer 2,7-(aminomethyl)naphthoic acid (2,7-Amn) spacer (**5**) leads to either a decrease or a complete loss of activity towards $\alpha_v\beta_3$ and $\alpha_v\beta_5$, respectively. The dramatic increase in activity observed for the Mamb containing compound **1** as compared to either unconstrained linear **7** or the rigid 2,7-Amn-containing **5** supports the hypothesis that the RGDDV pharmacophore binds to $\alpha_v\beta_3$ in a unique conformation.

The best linker to constrain the RGDY(Me)R pentapeptide sequence was obtained by cyclizing the side chain of a *C*-terminal glutamic acid residue onto the *N*-terminus of the pharmacophore (c[RGDY(Me)RE]-NH_2, **2**). This linker contains four freely-rotating bonds. As seen for the RGDDV sequence, constraining the pharmacophore with the 2,7-Amn linker (**6**) results in complete loss of activity at the $\alpha_v\beta_3$ receptor.

As part of the program to design peptidomimetic antagonists to integrin $\alpha_v\beta$, the conformations in solution of cyclic peptides that contain the two pharmacophores have been investigated. Using ^{1}H-NMR spectroscopy and molecular modeling, specific conformations are found in solution which confirm existing models for RGD-containing peptides [8,17–25]. There is solid evidence that the binding site of the $\alpha_v\beta_3$ receptor is narrower and more compact compared to that of $\alpha_{IIb}\beta_3$. Ligands that selectively bind $\alpha_v\beta_3$ adopt conformations with distances of less than 6 Å between the C^β atoms of the Arg and Asp residues within the RGD sequence, while ligands that bind $\alpha_{IIb}\beta_3$ exhibit more extended conformations with distances of 7–8 Å [9,10,26,27]. Our studies correlate the distances between the C^β atoms of Arg and Asp with the turn motif around the RGD sequence, the conformations of the DDV or DY(Me)R sequences, and the linker used in cyclization.

It is assumed that the 3-D orientation of the RGD sequence bound to $\alpha_v\beta_3$ is similar in both pharmacophores. Therefore, it can be assumed that conformations about the RGD portion found in common between the two pharmacophores are responsible for binding.

MATERIAL AND METHODS

Peptide Syntheses

The peptides were synthesized at Integra LifeSciences Corporation, Corporate Research Center, by methods previously reported [16]. Their preparation and biological characterization will be reported elsewhere.

Table 1 Activities of RGD-Containing Peptides at the Integrin Receptors[a,b]

Entry	Sequence[c]	VN/$\alpha_v\beta_3$ ELISA IC_{50} (μM)[d]	VN$\alpha_v\beta_5$ ELISA IC_{50} (μM)[d]	FN/$\alpha_5\beta$ ELISA IC_{50} (μM)[d]	Platelet aggregation IC_{50} (μM)[e]
1	c[RGDD(*t*-BuG)(Mamb)]	0.0006	0.014	0.042	14
2	c[RGDY(Me)RE]-NH_2	0.0036	10	0.43	0.82
3	c[RGDDV(Mamb)]	nt[f]	nt	nt	nt
4	c[MpaRGDD(*t*-BuG)C]-NH_2	0.006	0.55	0.32	26
5	c[RGDD(*t*-BuG)(2,7-Amn)1	0.017	10	nt	nt
6	c[RGDY(Me)R(2,7-Amn)]	25	>10	nt	nt
7	AcRGDDVG-NH_2	1.6	nt	nt	nt
8	c[MpaRGDDVC]-NH_2	0.024	3.0	1.2	77

[a] Reference [11].
[b] Abbrevations: VN, vitronectin; FN, fibronectin; *t*-BuG, *tert*-butylglycine; Mamb, *m*-aminomethylbenzoic acid; Y(Me), *o*-methyltyrosine; Mpa, 3-mercaptopropionic acid; 2,7-Amn, 2,7-aminomethylnaphthoic acid; Ac, acetyl.
[c] Residues in brackets are contained either in an end-to-end lactam (**1**,**3**,**5**,**6**) or in an *N*-terminal to side chain lactam (**2**) or in cyclic disulfides (**4**,**8**).
[d] Competitive ELISA, ligand/receptor.
[e] Platelet aggregation in platelet rich normocalcemic plasma (heparin) induced by ADP (10 μM). Platelet aggregation is a cell-haled assay that measures affinity to integrin $\alpha_{IIb}\beta_3$.
[f] The script nt stands for result not tested.

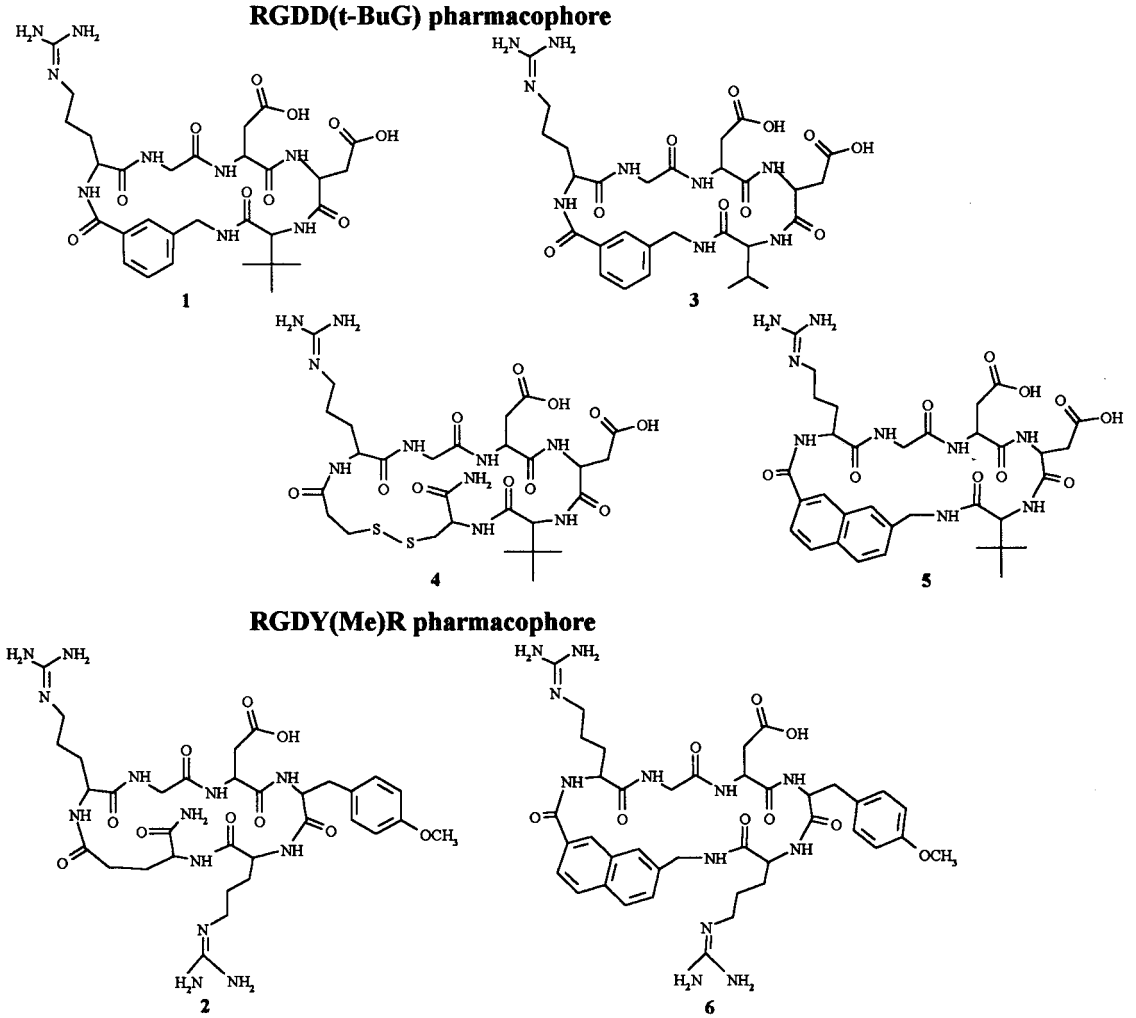

Scheme 1 Sequence of the cyclic peptides examined.

Binding Assays

Inhibition assays (IC_{50}) were carried out at Integra LifeSciences Corporation, Corporate Research Center, as previously reported [16].

NMR Spectroscopy

The samples were dissolved in 90% H_2O/10% D_2O (pH ~ 5) and in DMSO-d_6 purchased from Isotec Inc. at concentrations $\approx$ 5 mM. All ^1H NMR spectra were measured on a Bruker AMX 500 spectrometer operating at 500 MHz. The 1D spectra of 16–32 K data points were acquired at temperatures between 290 and 315 K in order to measure the NH temperature coefficients. The 2D-NMR spectra were acquired at 273 K in water solution to improve the nuclear Overhauser effect (NOE) and at 300 K in DMSO-d_6.

Depending on the experimental sensitivity, a variable number of scans in the range between 64 and 144 was acquired for each t_1 increment and 450–512 t_1 increments were collected from 2 K data points. Acquisition was performed in the phase sensitive mode using the time proportional phase increment method (TPPI). Free induction decays were multiplied by appropriate window functions in both time domains and zero filled to 2 K $\times$ 2 K real points.

The water signal was suppressed by irradiation with a selective gated pulse during the relaxation delay. In the case of nuclear Overhauser effect spectroscopy (NOESY) irradiation was also applied during the mixing time. The carrier frequency was placed at the frequency of water resonance spanning a spectral width of 5500 Hz. In the case of DMSO-d_6 solutions, the carrier frequency was set in

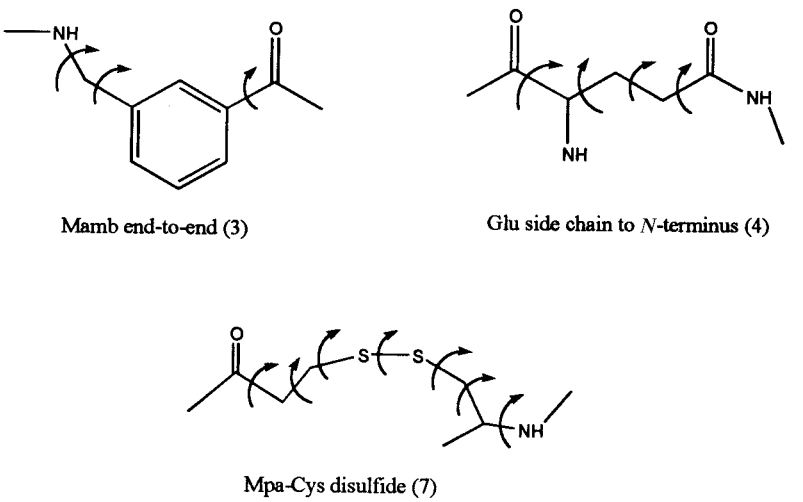

Scheme 2 Diagram of the freely rotating bonds (in parentheses) for each of the linkages used.

the middle of the spectral window covering a spectral width of 7000 Hz.

Chemical shift assignments were obtained in a straightforward manner [28] by the combined used of DQF-COSY [29–31] and NOESY [32] experiments. Peak positions were measured relative to tetramethylsilane (TMS) in H_2O and relative to the residual solvent peak in DMSO-d_6 ($\delta = 2.49$ ppm) as internal standards.

The TOCSY [33] experiments were acquired using the MLEV-17 spin-lock sequence typically at a field strength of 10 kHz for a total mixing time of 75–80 ms. NOESY spectra were conducted with a mixing time of 200 and 300 ms. Because the NOEs at the experimental conditions were positive and moderately intense it was not necessary to use rotating frame techniques to characterize the peptide conformations. ROESY [34] spectra were used to verify the presence of exchange cross-peaks when they appeared. In this case a spin-locking field of 2.5 KHz was used.

Cross-peak volumes of the NOESY spectra were integrated using the Felix software [35]. The values thus obtained were converted into interproton distances using fixed geometrical distances. Usually, the distance of 1.78 Å for the Gly^2 α_1/α_2 or the Asp^3 β_1/β_2 were taken as references in both the amide and aliphatic regions. On the basis of the comparison with other covalent distances, an error of ± 0.5 Å was estimated. Thus, NOEs were included in the molecular modeling calculations as intervals of distances between pair of atoms: upper and lower limits were set to the measured distance ± 0.5 Å.

Stereospecific assignment of the C$^\beta$H resonances for Asp and Y(Me) residues in the sequences was accomplished by the combination of β-proton to backbone proton NOEs and α-β proton coupling constants as described by Yamazaki *et al.* [36]. The $^3J_{NH,\alpha}$ and $^3J_{\alpha,\beta}$ coupling constants were obtained by 1D spectra and are displayed in Table 2. Data missing are due to either spectral overlap or line broadening of the resonances. Additional stereospecific β-proton assignments, as in the case of the arginine sidechain, were not possible because of ambiguities in the interpretation of 1H NOEs and coupling constants. The $^3J_{\alpha,\beta}$ coupling constants were used to calculate the side chain populations. For the calculations of aliphatic amino acids, Pachler's Equations [37] were used while Cung's Equations [38] were used for aromatic residues. The side chain populations for peptides c[RGDD(*t*-BuG)(Mamb)] (**1**), c[RGDY(Me)RE]-NH_2 (**2**) and c[RGDDV(Mamb)] (**3**) are discussed.

Molecular Modeling

Molecular simulations were used to search for the conformational preferences of the molecules in DMSO-d_6 and aqueous media. All molecular modeling calculations were carried out on a Silicon Graphics Iris Indigo. The computational protocol included distance geometry (DG), energy minimizations (EM), molecular dynamics (MD) and cluster analysis. All the NMR data available, including NOEs, coupling constants and information about the NH proton-shielding were taken into account.

Table 2 Temperature Coefficients (ppb/K) and Vicinal Coupling Constants[a] $^3J_{NH,\alpha}$ (Hz), $^3J_{\alpha\beta}$ (Hz) Determined in H_2O and DMSO-d_6 Solutions for the RGD-Containing Peptides

Entry	Residue	$\lvert\Delta\delta_{NH}/\Delta T\rvert$		$^3J_{NH,\alpha}$		$^3J_{\alpha,\beta}$	
		H_2O	DMSO	H_2O	DMSO	H_2O	DMSO
1	Arg[1]	7.6	5.9	7.1			
	Gly[2]	7.1	5.9	$4.0_l/6.2_h$	$6.4_l/4.2_h$		
	Asp[3]	8.5	1.6	7.9	8.5	$4.5_l/8.2_h$	
	Asp[4]	2.8	5.8	6.2		$8.8_l/4.9_h$	
	(*t*-BuG)[5]	7.4	0.5	6.4	7.9		
	(Mamb)[6]	6.8	5.7	6.1	3.7_h		
2	Arg[1]	4.4	2.2	8.1			
	Gly[2]	8.0	8.0	$4.2_l/6.3_h$	4.6_l		
	Asp[3]	9.5	6.9	7.6	7.7	$4.5_l/8.7_h$	$4.1_l/9.5_h$
	Y(Me)[4]	5.1	1.9	7.8	8.5	$5.4_l/9.7_h$	$10.7_l/3.2_h$
	Arg[5]	9.4	5.4	3.7	3.8		
	Glu[6]	9.2	5.5	7.6	8.3		
3	Arg[1]	9.4	3.6	9.3			
	Gly[2]	7.8	5.8	$3.5_l/6.0_h$	$5.7_l/4.6_h$		
	Asp[3]	7 9	2.5	7.7	8.7	4 $4_l/8.1_h$	
	Asp[4]	2.6	3.7	6.2	$9.3_l/4.4_h$		
	Val[5]	10.3	2.4	6.0	6.9		
	(Mamb)[6]	9.5	5.4	$5.6_l/5.8_h$	$7.2_l/4.4_h$		
4	Arg[1]	3.4	4.3	6.7			
	Gly[2]	8.1	7.1	$4.6_l/5.0_h$	$6.0_l/4.4_h$		
	Asp[3]	7.1	0.3	8.2	7.0		
	Asp[4]	6.8	5.6	6.7			
	(*t*-BuG)[5]	6.4	0.5	8.2	9.0		
	Cys[6]	8.7	5.4	8.1	8.3		
5	Arg[1]	4.7	0.4	7 9	7.3		
	Gly[2]	7.3	6.6	$2.9_l/6.4_h$	$5.1_l/5.6_h$		
	Asp[3]	7.0	6.1	9.2	8.1	7.5_h	7.7_h
	Asp[4]	5.4	0.7	4.4	5.8	$11.0_l/2.9_h$	4.2_h
	(*t*-BuG)[5]	7.1	7.0	7.4	8.5		
	(2,7-Amn)[6]	10.9	5.0		$7.4_l/4.7_h$		
6	Arg[1]	4.2	7.0	6.2			
	Gly[2]	10	4.8	$4.8_l/4.9_h$			
	Asp[3]	8.0	2.0	8.1		$5.3_l/7.0_h$	
	Y(Me)[4]	2.0	0.7	6.2		$6.0_l/5.9_h$	
	Arg[5]	7.1	5.2	5.1			
	(2,7-Amn)[6]	12	7.0				

[a] The subscripts l and h denote low and high field resonances, respectively.

The conformational space was searched by distance geometry (DG) as implemented in the software package NMRchitect [39]. Qualitative analysis of the NOE patterns indicates that all peptide bonds adopt a *trans* conformation as noted by the absence of $C^{\alpha}H(i)$-$C^{\alpha}H(i+1)$ and $NH(i)$-$C^{\alpha}H(i+1)$ correlations. Thus, during the molecular modeling simulations the peptide bonds were kept in the *trans* structure. Around 500 structures were stored for each peptide consistent with the NMR data.

The ϕ torsional angles and hydrogen bonding patterns were used to filter out structures that did not fit the experimental data. Torsional angle constraints were included in the form of $^3J_{NH,\alpha}$ which is related to the backbone dihedral angle ϕ according to a generalized form of the Karplus expression [40,41]. The acceptable boundary for the use of vicinal coupling constants was ± 2 Hz, both in the conformational search and in the selection of energy-minimized conformers. In the case of hydrogen

bond based selection, only structures were retained in which the NH protons, showing an absolute value of the temperature coefficients < 3 ppb/K, are involved in an effective hydrogen bond. A hydrogen bond was valued on the basis of the distance r_{AD} (≤ 3.2 Å) and the angle $\theta_{A\text{-}H\text{-}D}$ ($\leq 35°$) where A and D are the acceptor and the donor heavy atoms, respectively. The remaining structures were subjected to energy minimization and molecular dynamics (MD) with the Discover program [42]. The calculations were performed *in vacuo* applying the CVFF force field. A distance dependent dielectric constant was used for the nonbonded interactions to approximate solvation. The NOE restraints were included (when indicated) with a force constant of 20 Kcal (mol·Å^2). For minimizations the VA09A algorithm was used until the maximum derivative was less than 0.01 Kcal/mol. The energy cutoff was 30 Kcal above the minimum. The DG minimized structures were clustered based upon backbone heavy atom superposition (RMSD ≤ 0.5) or backbone torsional angles (ϕ, $\psi \pm 20°$). Each cluster contained between 20–60 structures. The lowest energy member of each cluster was used for subsequent analysis. Prior to every molecular dynamic simulation the system was equilibrated with 10 ps initialization dynamics. The MD studies were performed at 300 K with a time step of 1 fs over a simulation time of 500–1000 ps with snapshots recorded each picosecond. These MD trajectories were analyzed to delineate peptide backbone motions. Specifically, Arg^1C^β-Asp^3C^β distances were focused on of all the conformations monitored during 500 ps of restrained molecular dynamics simulations.

Another protocol for the molecular modeling simulations was run independently giving comparable results. In the second procedure, conformations were generated by searching torsional angle space with the Monte Carlo multiple minimum (MCMM) procedure as implemented in the MacroModel program. The Merck Molecular Force Field with full atomic charges was used with the GB/SA solvation model for water. Two long conformational searches were run. The first with no constraints to generate an ensemble of low energy conformers. A second simulation was then run with three strong NOE constraints which were found in both the water and in the DMSO NMR data to bias the search towards conformers that fit the NMR data. For each run between 150 and 350 low energy conformations were stored, and the energy cut-off was 30 kcal above the minimum. These conformations then were filtered and clustered based upon subsets of the NOE or H-bonding data. All filtered conformations were relaxed by simulated annealing before full minimization and analysis by molecular dynamics.

RESULTS

A mono-conformational analysis which relies on a single structure to explain all the NMR data available is not often accurate for small molecules in solution even if they are constrained by cyclization. However, this approach can be useful to define highly populated conformations. In order to explore the conformational space accessible in solution the results obtained were compared for several analogs sharing the same pharmacophores in polar (H_2O) and less polar (DMSO) environments.

Simulations by molecular modeling show that several conformations are present in solution. The NMR spectra of all the molecules, except for the c[RGDY(Me)R(2,7-Amn)] (**6**), exhibit only one set of resonances indicating that the conformers exchange faster than the timescale of the NMR experiments. All the conformations obtained by computer simulations are well characterized and consistent with the spectroscopic data.

Detailed descriptions of the conformations and results of the molecular dynamics simulations of the peptides c[RGDD(*t*-BuG)(Mamb)] (**1**) and c[RGDY(Me)RE]-NH_2 (**2**) are presented. Brief summaries of the conformational studies for the other four peptides are reported. Based upon these data structural features of the two pentapeptide pharmacophores relevant for inhibitory activity are proposed. In Figure 1 a pseudo-plane established by the type I β-turn with the Arg in the $i+1$ position is displayed for c[RGDD(*t*-BuG)(Mamb)] (**1**). This figure illustrates the axial/up (ax/up), axial/down (ax/down) and equatorial/out (eq/out) orientations with respect to the pseudo-plane. In all molecules the amino acids are numbered as follows: $R^1G^2D^3X^4X^5$.

tert-Butylglycine, m-(Aminomethyl)benzoic acid RGD-analog: c(RGDD(t-BuG)Mamb) (1). For this compound two different highly populated conformations are obtained dependent on whether the NMR data in water or those in DMSO-d_6 are used. In each case, the structure obtained is fully consistent with the NMR data including the NH temperature coefficients. The main difference between these two conformations is the location of the β-turn within the RGD sequence.

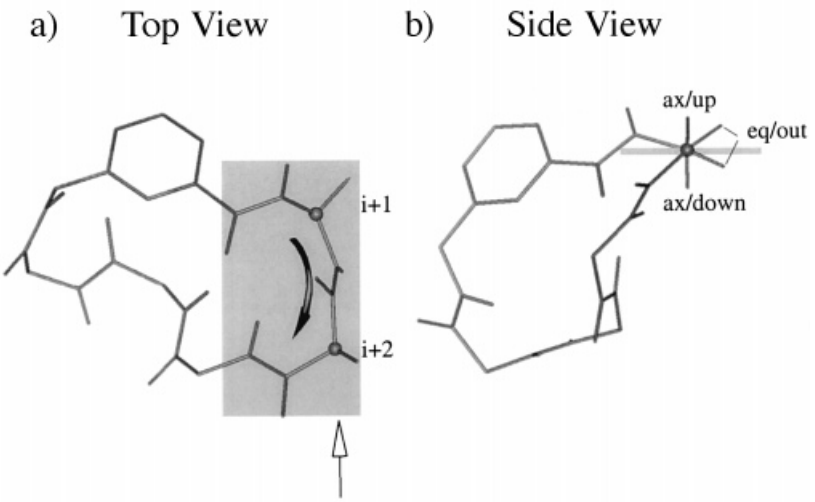

Figure 1 (a) Representation of the pseudo-plane defined by a type I β-turn with the Arg in the $i+1$ position for the c[RGDD(t-BuG)(Mamb)] (**1**) sequence. Only the backbone atoms of the molecule are displayed. The filled arrow indicates the orientation of the β-turn and the vertical arrow indicates the axis for the side-view projection. (b) Projection along the $C^{\alpha}(i+1)$–$C^{\alpha}(i+2)$ indicating the axial/up (ax/up), axial/down (ax/down) and equatorial/out (eq/out) positions relative to this axis.

The conformer populated in DMSO-d_6 adopts a type I β-turn with Arg^1 in the $i+1$ position and a γ-turn about Asp^4 (Figure 2(A) and (B)). This arrangement is stabilized by the NH(3)-CO(6) and the NH(5)-CO(3) hydrogen bonds. The low temperature-dependence of the amide protons of residues in position 3 and 5 (Table 2 entry 1), sequential NH-NH NOEs around the RGD segment and medium range connectivities $C^{\alpha,\beta}H(1)$-NH(3) and $C^{\beta}H(3)$-NH(5) (Figures 3 and 4(a)) define the consecutive βI/γ-turn arrangement. However, not all NOEs observed in DMSO-d_6 are consistent with this conformation. Specifically, the NH(3)-NH(4) and $C^{\alpha}H(2)$-NH(4) NOEs are consistently violated and agree with the presence of a second conformer in solution with a β-turn centered around the Gly^2-Asp^3 dipeptide.

For the NMR data obtained in H_2O the major conformation adopts a type II′ β-turn in which Gly occupies the $i+1$ position (Figure 2(C) and (D)). The NH(3)-NH(4) and $C^{\alpha}H(2)$-NH(4) proximities supporting the β-turn are considerably stronger than in DMSO-d_6 solution and represent the only informative backbone NOEs involving the RGDD sequence (Figure 4(a)). This particular arrangement is also consistent with the low temperature-dependence determined for the Asp^4NH (Table 2 entry 1), which is the only NH shielded from the solvent. Analysis of the trajectories during molecular dynamics shows that the conformation of the β-turn is slightly distorted. The particular hydrogen bond is not populated throughout the whole MD simulation and the carbonyl oxygen of Arg^1 is also involved in a y-turn (bifurcation), as commonly observed in βII′-turns. The major backbone conformation in water also appears accessible in DMSO-d_6 even though it is less populated.

In H_2O the $^3J_{\alpha,\beta}$ coupling constants of Asp^3 (4.5_l/8.2_h) and Asp^4 (8.8_l/4.9_h) (Table 2 entry 1) indicate that averaging between different rotamers for the side chains occurs. However, calculated side chain conformers using Pachler s Equations [37] show that for each residue the *gauche* (–) rotamer ($\chi_1 = -60°$) predominates. In DMSO-d_6 the β-proton resonances are either coincident or not well resolved for spectral overlap with the solvent or line-broadening to determine the $^3J_{\alpha,\beta}$ coupling constants.

Visual inspection of the superposition of the heavy atoms suggests that the vectoral and spatial relationships of the Arg^1, Asp^3, Asp^4, and t-BuG^5 side chains differ between the two turn arrangements found in DMSO-d_6 and water. Furthermore, for each β-turn array two different conformations are observed defined by the location of the side chains in axial or equatorial quadrants.

In the type I β-turn ensemble found in DMSO the Arg^1 side chain adopts the eq/out conformation while the Asp^3 side chain occupies the ax/up conformation. The latter side chain orientation is consistent with the $C^{\beta}H(3)$-NH,ϕH(6) NOEs, where ϕH

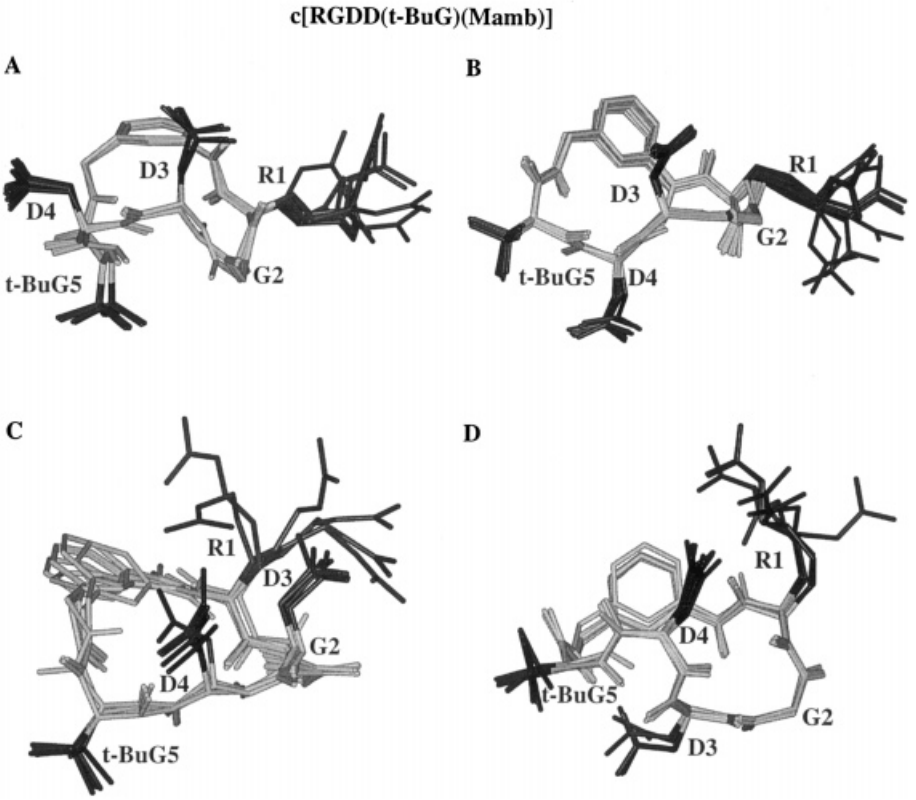

Figure 2 View of the overlay of the ensembles of structures found for c[RGDD(*t*-BuG)(Mamb)] (**1**) in DMSO-d_6 showing the β-turn about the Arg^1-Gly^2 dipeptide and in aqueous solution showing the β-turn about the Gly^2-Asp^3 dipeptide. A: Asp^4 and *t*-BuG^5 side chains in the ax/up and ax/down quadrants. B: Asp^4 and *t*-BuG^5 side chains in the ax/down and eq/out quadrants. C: Asp^3 side chain in the ax/up quadrant. D: Asp^3 side chain in the eq/out quadrant.

is the aromatic proton in position 2, *ortho* to the two substituents of the benzene ring. In this conformation, the Asp^4-(*t*-BuG)^5 dipeptide sequence is flexible. The Asp^4 and *t*-BuG^5 side chains are either in the ax/up and ax/down quadrants, respectively (Figure 2(A)) or they have interchanged positions and the Asp^4 side chain is ax/down and the *t*-BuG^5 is eq/out (Figure 2(B)). There is experimental evidence for both orientations encountered for Asp^4, such as the observation of $C^{\gamma}H(4)$-NH(6) and $C^{\beta}H(4)$-NH(6) NOEs.

In the second backbone conformation the β-turn is shifted by one amino acid and is now centered at Gly^2-Asp^3. As a consequence, the Arg^1 side chain is raised into the ax/up quadrant. The Asp^3 residue is found either in the ax/up (Figure 2(C)) or in the eq/out (Figure 2(D)) quadrants. Finally, in both arrays, the Asp^4-(*t*-BuG)^5 dipeptide sequence is found in a conformation with the Asp^4 side chain in the ax/up quadrant and the *t*-BuG^5 side chain in the eq/out. This side chain orientation is consistent with the NOE connectivities between $Asp^4C^{\beta}H$ and either $Mamb^6NH$ or ϕH, the aromatic proton in position 2 of the benzene ring.

O-Methyltyrosine*, N-*terminal to side chain lactam RGD-analog: c(RGDY(Me)RE)-NH_2 (2). The analysis of the minimized structures reveals the presence of only one defined β-turn arrangement centered around Gly^2-Asp^3 in the RGD sequence (Figure 5). This structure is supported by the temperature-dependence of the amide protons which is similar in H_2O and DMSO-d_6 (Table 2 entry 2). There is no evidence of the involvement of the NH protons in aqueous solution in a stable hydrogen bond. However, the lowest temperature coefficients found are for Arg^1 NH and $Y(Me)^4$ NH in both solvents. A strong NH(3)-NH(4) connectivity between the $i+2$ and $i+3$ residues of the turn and a $C^{\alpha}H(2)$-NH(4) connectivity between the $i+1$ and $i+3$ residues of the turn are found in both solvents to define the

position of the β-turn (Figure 4(b)). Furthermore, the low-temperature-dependence of the Tyr^{4}NH in DMSO-d_6 (Table 2 entry 2) supports the presence of a hydrogen bond stabilizing this turn.

A further inspection of the structures suggests the presence of a hydrogen bond between the Asp^{4}CO and Arg^{1}NH, which results in a turn centered on Arg^5-Glu^6. Both the low temperature coefficient of Arg^{1}NH found in DMSO-d_6 and the small $^3J_{NH/\alpha}$ coupling constant (<4 Hz) of Arg^5 (Table 2 entry 2) are indicative of a non-extended structure.

The Asp^3 and Y(Me)^4 side chains adopt predominantly orientations characterized by a χ^1-angle of $-60°$ as indicated by the $^3J_{\alpha\beta}$ coupling constants in combination with the stereospecific assignments of the β-protons.

MD simulations indicate that the conformation with two β-turns is not rigid but undergoes a rotation of the amide plane between Y(Me)^4-Arg^5. As a consequence, the H-bond acceptor Y(Me)^{4}CO is turned outside the ring and the H-bond is broken. This finding is supported by some medium and long-distance NOEs involving the Arg^5 amide proton (Figure 4(b)) such as the NH(4)-NH(5) and the NH(5)-NH(1) connectivities which clearly support an internal orientation of the Arg^5 amide proton with respect to the backbone ring.

An analysis of the heavy atom superposition of the minimized structures reveals that the orientation of the Asp^3 side chain is well defined and occupies the ax/up position (Figure 5). However, the Arg^1 residue and the Y(Me)^4-Arg^5 sequence are found to be flexible, and three orientations are observed. The first one is similar to that found for the Mamb-containing **1** depicted in Figure 2(C). The Arg^1 occupies the ax/up quadrant while the Y(Me)^4-Arg^5 side chains are arrayed ax/up-eq/out, respectively (Figure 5(A)). The second side chain array has the same ax/up-eq/out orientation of the Y(Me)^4-Arg^5 dipeptide as the first one. However, the Arg^1 side chain has undergone a 180° rotation and is found in the ax/down position (Figure 5(B)). Experi-

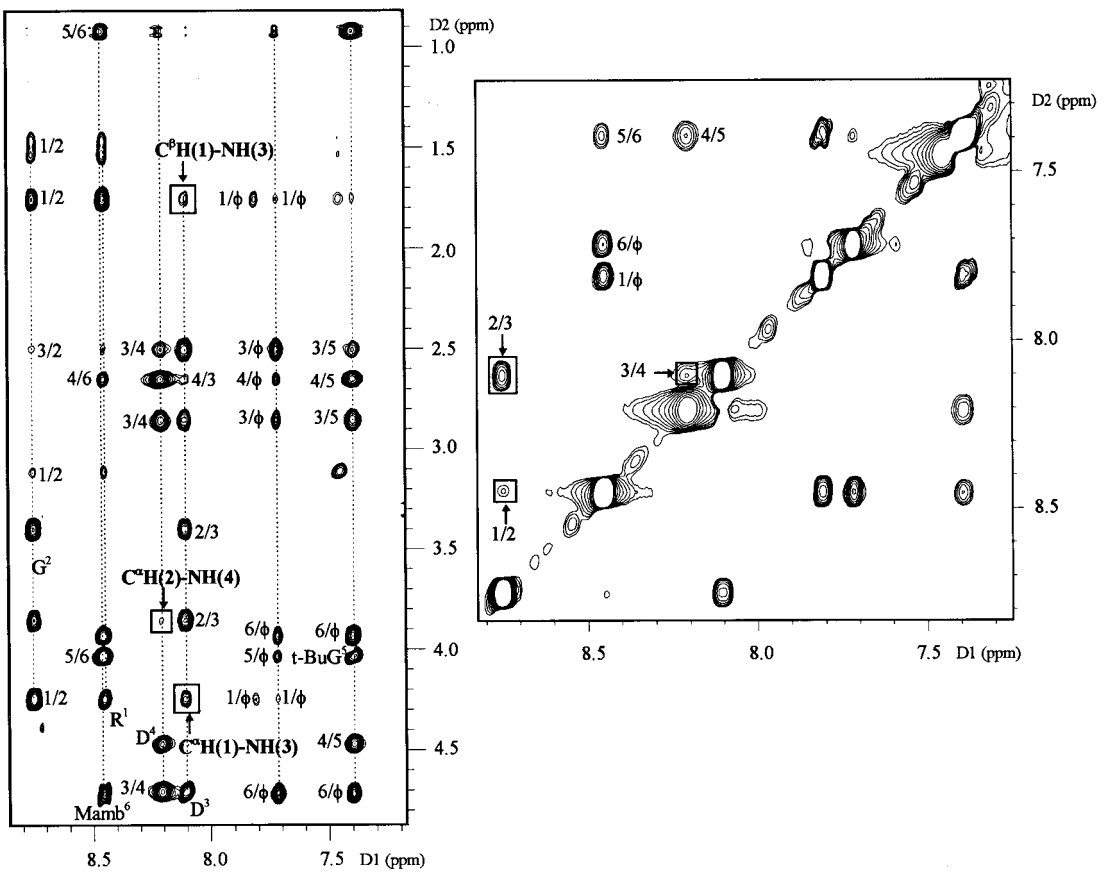

Figure 3 Portions of a NOESY spectrum of c[RGDD(*t*-BuG)(Mamb)] (**1**) at 300 K in DMSO-d_6. Sequential NH$\rightarrow$NH and $i\rightarrow i+2$ connectivities are indicated.

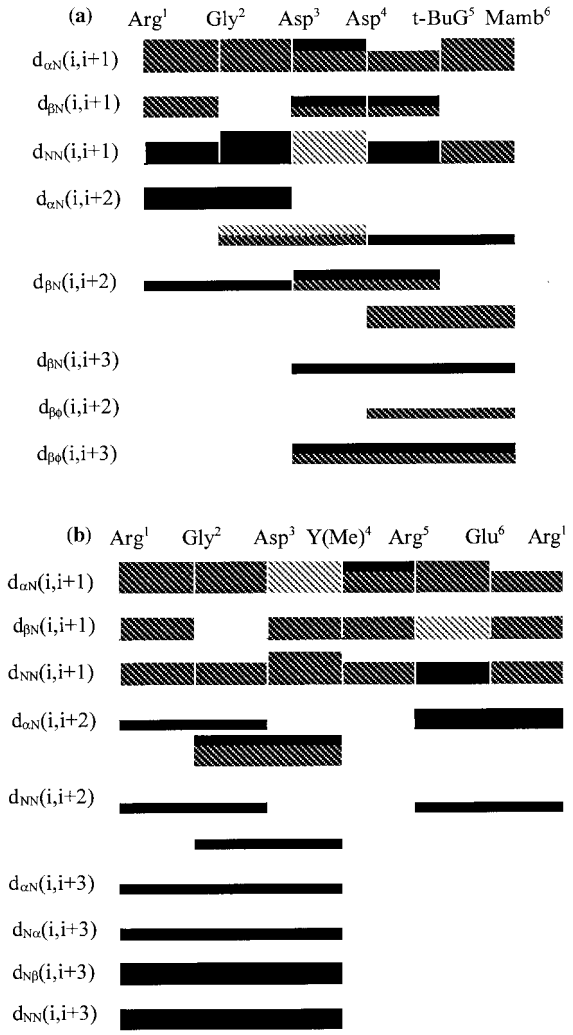

Figure 4 Interresidue NOEs determined in DMSO-d_6 and aqueous solution for (a) c[RGDD(*t*-BuG)(Mamb)] (**1**) and (b) c[RGDY(Me)RE]-NH2 (**2**). NOE intensities are displayed as for values determined in DMSO, as for values determined in H_2O and as for values determined in both solvents, and are classified as weak (3.5–5.0 Å), medium (2 8–3.5 Å) and strong (< 2.8 Å).

mentally, this side chain orientation of Arg^1 is supported by the $C^{\gamma}H(1)$-NH(4) NOE. In the third possible side chain topology, the side chain of Arg^1 is eq/out, and those of the Asp^3-$Y(Me)^4$-Arg^5 sequence are in an up/down/up orientation similar to a β-strand (Figure 5(C)). There is experimental evidence for both side chain orientation of the $Y(Me)^4$ ax/up and ax/down such as the observation of $C^{\gamma}H(4)$-NH(1) and $C^{\beta}H(4)$-NH(1) NOEs.

Valine, m-(Aminomethyl)benzoic acid RGD-analog: c(RGDDV(Mamb)) (3). This compound exhibits similar H-bonding patterns (Table 2 entry 3) and NOE proximities (Figure 6(a)) as c[RGDD(*t*-BuG)(Mamb)] (**1**). However, it shows a higher flexibility in DMSO-d_6 and does not adopt a predominant conformation.

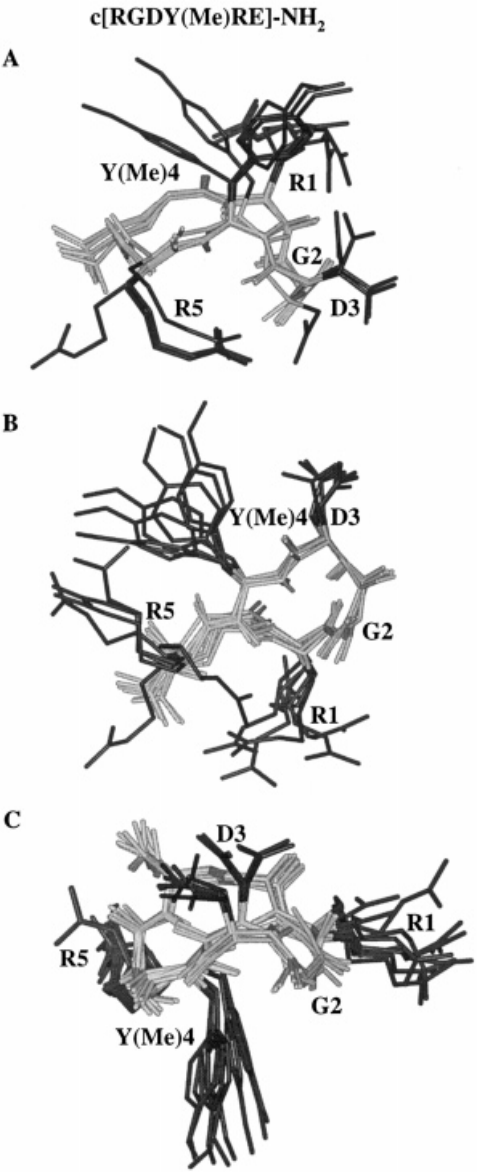

Figure 5 View of the overlay of the ensembles of structures found in aqueous solution for c[RGDY(Me)RE]-NH_2 (**2**) showing the β-turn about the Gly^2-Asp^3 dipeptide. A: Arg^1 side chain in the ax/up quadrant and $Y(Me)^4$-Arg^5 side chains in the ax/up-eq/out orientation. B: Arg^1 side chain in the ax/down position and $Y(Me)^4$-Arg^5 side chains in the ax/up-eq/out orientation. C: Arg^1 side chain in the eq/out position and $Y(Me)^4$-Arg^5 side chains in the ax/down-ax/up orientation.

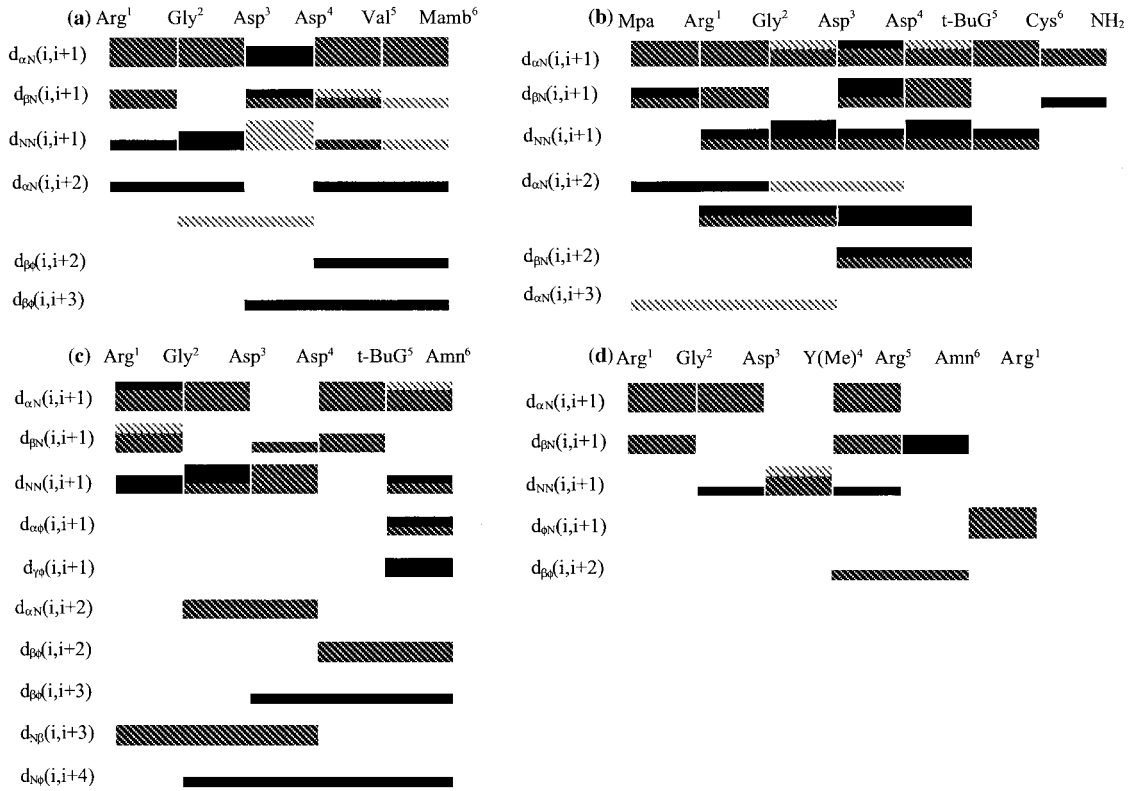

Figure 6 Interresidue NOEs determined in DMSO-d_6 and aqueous solution for (a) c[RGDDV(Mamb)] (**3**), (b) c[MpaRGDD(*t*-BuG)C]-NH_2 (**4**), (c) c[RGDD(*t*-BuG)(2,7-Amn)] (**5**) and (d) c[RGDY(Me)R(2,7-Amn)] (**6**). NOE intensities are displayed as ▭ for values determined in DMSO, as ▨ for values determined in H_2O and as ▧ for values determined in both solvents, and are classified as weak ▭ (3.5–5.0 Å), medium ▭ (2.8–3.5 Å) and strong ▭ (< 2.8 Å).

This is indicated by the medium temperature-dependence of the Asp^3, Asp^4 and Val^5 amide protons which indicate partial involvement in a H-bond. This result is not surprising as the incorporation of the Val residue instead of the *t*-BuG allows a more flexible structure.

The *t*-BuG in c[RGDD(*t*-BuG)Mamb] (**1**) was replaced with Val to determine whether the side chain of the residue in that position has a preferred orientation. Because *t*-BuG does not have a β-proton, preferred rotations about the C^α to C^β bond from $^3J_{\alpha,\beta}$ coupling constants cannot be determined. Unfortunately, in the 1D spectrum of c[RGDDV(-Mamb)] (**3**) the ValC^βH resonances appear as an unresolved multiplet and the ValC^αH resonance appears as a simple triplet. Therefore, it was not possible to distinguish between the $^3J_{NH,\alpha}$ and $^3J_{\alpha,\beta}$ coupling constants. Based upon the calculated population of the side chain rotamers from the $^3J_{\alpha,\beta}$ coupling constants in H_2O, both Asp^3 and Asp^4 side chains adopt predominantly the g^- rotamer. The g^- rotamer of these residues is also the preferred one in aqueous solution for c[RGDD(*t*-BuG)(Mamb)] (**1**). $^3J_{\alpha\beta}$ coupling constants in DMSO-d_6 are not determinable from the 1D spectrum as already observed for analog **1**.

3-Mercaptopropionic acid, tert-Butylglycine RGD-analog: c(MpaRGDD(t-BuG)C)-NH_2 (4). In aqueous solution this peptide is found to be quite flexible, which is expected based upon greater flexibility of the disulfide linkage. No amide protons are found to be solvent shielded (Table 2 entry 4) and no strong sequential NH-NH connectivities are observed to define a well populated β-turn (Figure 6(b)). Evidence of a conformational equilibrium is provided by some inconsistences found in the NOE data. Specifically, the observation of both C^αH(1)-NH(3) and C^αH(2)-NH(4) NOEs cannot be satisfied by only one type of β-turn. Furthermore, molecular dynamics studies suggest that all conformations found for Mamb-containing **1** are energetically accessible.

In DMSO-d_6 similar hydrogen bonding and NOEs are observed as for compound **1** in this solvent. The conformational studies of disulfide **4** did not

result in new conformations for the RGDDV pharmacophore.

Compounds **1** and **4** which share the same pentapeptide pharmacophore adopt also the same ensemble of conformers in solution. However, compound **1** is one order of magnitude more potent towards the $\alpha_v\beta_3$ receptor than compound **4**. This result can be explained by the greater flexibility shown by molecular modeling of compound **4** probably due to the disulfide cyclization.

Two end-to-end cyclic peptides were studied in which the Mamb linker is replaced by 2,7-(aminomethyl)naphthoic acid (2,7-Amn). 2,7-Amn is a longer linker than Mamb. The distance between N–$\underline{C}^{\alpha}H_2$ and the carboxyl groups ϕ-$\underline{C}O$ is $\approx$7.5 Å in the 2,7-Amn residue while it is $\approx$5.0 Å in Mamb. The increased distance of the spacer did not result in new conformations for the two pharmacophores but instead is found to limit the proximity between the C^{β} atoms of Arg^1 and Asp^3.

tert-Butylglycine, 2,7-(Aminomethyl)naphthoic acid RGD-analog: c(RGDD(t-BuG)(2,7-Amn)) (5). The NMR data in DMSO-d_6 for this molecule show similarities with c[RGDY(Me)RE]-NH_2 (**2**). In both compounds the amide protons of residues at positions 1 and 4 have the smallest temperature coefficients corresponding to an effective shielding from the solvent (Table 2 entries 2 and 5). During molecular dynamics only Asp^4NH is effectively involved in a hydrogen-bond which is consistent with a type II′ β-turn about Gly^2-Asp^3. This arrangement is well defined as the hydrogen-bond is populated throughout the whole simulation. The experimental data are consistent with the ensemble of structures found. Specifically, the II′ β-turn motif is supported by the NH(3)-NH(4) and C^{α}H(2)-NH(4) NOEs (Figure 6(c)).

No well defined structure could be determined in aqueous solution. In fact, some NH(i)-NH($i+1$) and long distance NOEs are either missing or weaker than in DMSO-d_6 solution. Furthermore, no hydrogen-bond selection could be applied because of the high temperature-dependences of the NH chemical shifts (Table 2 entry 5).

The heavy-atom superposition of the minimized structures is reported in Figure 7. Residue Arg^1 and dipeptide Asp^4-(t-BuG)^5 are found in the same conformation as in the Mamb-analog (1) in aqueous solution (Figure 2(C) and (D)). The side chain orientation for the Asp^4 residue is defined by NOE connectivities between the β-protons of Asp^4 and both the Arg^1 NH and the aromatic protons of 2,7-Amn (positions 1 and 8 of the naphthalene moiety). The Asp^3 side chain is held in an eq/out orientation which causes the C^{β}-C^{β} distance between Asp^3 and

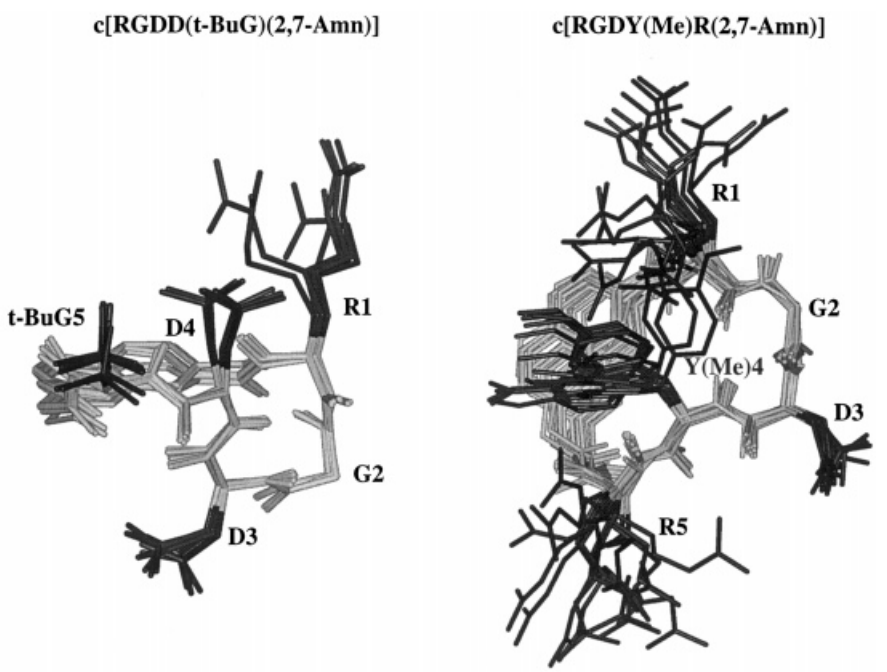

Figure 7 View of the overlay of the ensemble of structures found for c[RGDD(t-BuG)(2,7-Amn)] (**5**) in DMSO-d_6 (left) and for c[RGDY(Me)R(2,7-Amn)] (**6**) in aqueous solution (right) showing the β-turn about the Gly^2-Asp^3 dipeptide.

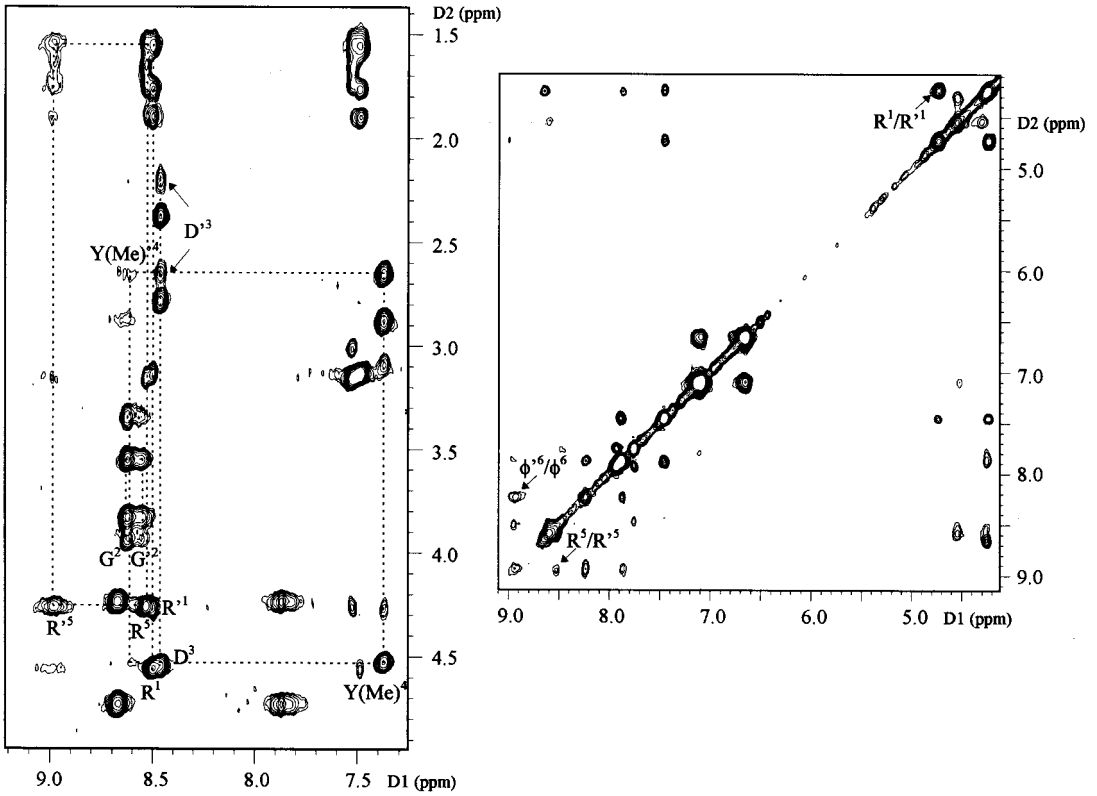

Figure 8 Portions of a TOCSY (left) and ROESY (right) spectrum of c[RGDY(Me)R(2,7-Amn)] (**6**) acquired in DMSO-d_6 at 300 K. Two sets of spin systems are indicated. In the ROESY spectrum only exchange cross-peaks are labelled.

Arg[1] to be considerably longer than 6 Å. The long distance between these side chains is probably responsible for the low activity of this peptide which is consistent with existing models for $\alpha_v\beta_3$ binding sites [9,10,26,27].

O-Methyltyrosine, 2,7-(Aminomethyl)naphthoic acid RGD-analog: c(RGDY(Me)R(2,7-Amn)) (6). The amide proton signals appear broad in both H_2O and DMSO-d_6 solution. Line broadening of the NH resonances did not allow the determination of the $^3J_{NH/\alpha}$ coupling constants. Furthermore, in DMSO-d_6 a minor set of resonances is present which corresponds to a second conformer in slow exchange, relative to the NMR time scale, with the predominant conformer. The equilibrium is fast enough to observe exchange cross-peaks between the two sets of resonances in the ROESY spectrum and in the fingerprint region of the TOCSY spectrum acquired with a mixing time of 80 ms. Specifically, Gly[2]NH-Gly[2]NH′ and Arg[5]NH-Arg[5]NH′ correlations enabled us to assign the spin system for these residues (Figure 8). These effects may arise from particular steric effects of the peptide ring together with geometrical requirements of 2,7-Amn. In aqueous solution the rate of exchange is fast on the NMR time scale and a second spin system can no longer be observed.

Molecular modeling results are consistent with the presence of a type II′ β-turn centered at Gly[2]-Asp[3]. The conformation of the β-turn is not well defined throughout the whole ensemble of structures. The particular hydrogen bond supporting the turn, Arg[1]CO-Y(Me)[4]NH, is only partially populated and the carbonyl oxygen of Arg[1] is also arranged in a γ-turn.

In both solvents the amide proton of Y(Me)[4] exhibits the lowest temperature-dependence (Table 2 entry 6) which indicates that this proton could be involved in the hydrogen bond forming the β-turn. In DMSO-d_6 the amide proton of Asp[3] is shielded from the solvent as well. This result either implies the existence of a different β-turn arrangement shifted by one residue as found for analogs containing the RGDDV pharmacophore, or supports the presence of the γ-turn about Gly[2] as suggested by molecular modeling. There are no other experimental data in DMSO-d_6 (Figure 6(d)) which can sup-

port the β-turn about Arg^1-Gly^2 or the γ-turn motif because the spectral overlap, especially of the α-proton resonances, does not allow proper assignments.

The homonuclear $^3J_{\alpha,\beta}$ coupling constants of Asp^3 ($5.3_l/7.0_h$) and Y(Me)^4 ($6.0_l/5.9_h$) in H_2O indicate that averaging may be occurring leading to a mixture of side chain rotamers. No data are available in DMSO solution.

In the predominant conformer obtained from MD calculations which exhibits a β-turn about Gly^2-Asp^3 (Figure 7) the orientations of the side chains of the pentapeptide are found to be similar to those described for c[RGDD(*t*-BuG)(2,7-Amn)] (**5**). Once again the Arg^{1}C$^\beta$-Asp^{3}C$^\beta$ distance is exceptionally long and could be responsible for the poor binding affinity to the $\alpha_v\beta_3$ receptor (Table 1).

DISCUSSION

As a starting point for the design of peptidomimetic antagonists to integrin $\alpha_v\beta_3$, the conformations were determined in a solution of two pentapeptide pharmacophores, the RGDDV and RGDY(Me)R sequences, that bind the receptor with high affinities and unique selectivities. The pharmacophores were constrained in cyclic peptides which are low–sub-nanomolar inhibitors of integrin $\alpha_v\beta_3$. By combining experimental NMR spectroscopy and molecular modeling studies, structural implications for activity are discussed. Common features in the conformational space accessible in solution for peptides containing the two pharmacophores are focused on as well as the reported preference for $\alpha_v\beta_3$ to bind the RGD sequence in a more compact conformation relative to $\alpha_{IIb}\beta_3$.

Comparison of the experimental data in H_2O and in DMSO-d_6 suggests that these molecules although constrained by cyclization do not exist in a single conformation but as a mixture of conformers in fast exchange on the NMR time scale. Broad NH signals, temperature-dependence of the NH resonances changing with the solvent and NOE patterns which cannot be explained by a single conformation experimentally support this conclusion. Despite these conformational transitions, the spectroscopic studies suggest conformations accessible in solution to all peptides under investigation which provide insight into common structural features. It is concluded that such common structures are the bioactive conformations.

Two backbone conformations are found for the pentapeptide pharmacophore in c[RGDD(*t*-BuG)(Mamb)] (**1**). There is evidence that the conformation found in H_2O is also accessible in DMSO-d_6 even though it is not the major structure. Each conformer is defined by the type and location of the β-turn in the RGD sequence. In contrast, only one β-turn conformation is observed for the pentapeptide pharmacophore within c[RGDY(Me)RE]-NH_2 (**2**). In the six peptides studied, the RGD sequence is found in only these two β-turn conformations.

It is assumed that the RGD seguence in both pharmacophores binds to the $\alpha_v\beta_3$ receptor in the same conformation. Since only the β-turn centered around Gly^2-Asp^3 is found to be common among both pharmacophores, we propose this β-turn to be relevant for inhibitory activity towards integrin $\alpha_v\beta_3$. In the conformations that contain this β-turn, only one is common to both pharmacophores. In this the Arg^1 and Asp^3 side-chains are in an ax/up orientation and both the Asp^4-(*t*-BuG)^5 and the Y(Me)^4-Arg^5 sequences have an ax/up-eq/out orientation (Figure 2(C) and Figure 5(A), respectively).

Based on common structural parameters between the RGDDV and RGDY(Me)R sequences within cyclic peptides it is possible to elucidate key elements of the pharmacophore models. Specifically, our analysis is focused on the orientation of surface-accessible hydrophobic and hydrophilic groups that are considered to be responsible for the desired biological activity. The pharmacophore models for the RGDD(*t*-BuG) and RGDY(Me)R sequences are reported in Plate 1. The spatial locations of hydrophobic and positive/negative ionizable groups are represented with spheres of different colors.

Previous structure activity studies with RGD containing peptides have indicated that the vectorial and spatial relationships of the charged sidechains of arginine and aspartic acid in the RGD sequence are critical for biological activity [9,10,26,27]. Arg^{1}C$^\beta$-Asp^{3}C$^\beta$ distances of all the structures are monitored during 500 ps of restrained molecular dynamics simulations. Only the conformations that are found to be accessible to both pharmacophores (Figure 2(C) and 5(A)) exhibit Arg^{1}C$^\beta$-Asp^{3}C$^\beta$ distances < 6 Å, which is believed to be a requirement for selective $\alpha_v\beta_3$ binding [9,10,26,27].

Compounds **1** and **4** which share the same pentapeptide pharmacophore exhibit different binding towards the $\alpha_v\beta_3$ receptor although conformations which adopt the optimal Arg^{1}C$^\beta$-Asp^{3}C$^\beta$ distance are accessible in solution for both peptides. The decrease in binding of compound **4** can be ex-

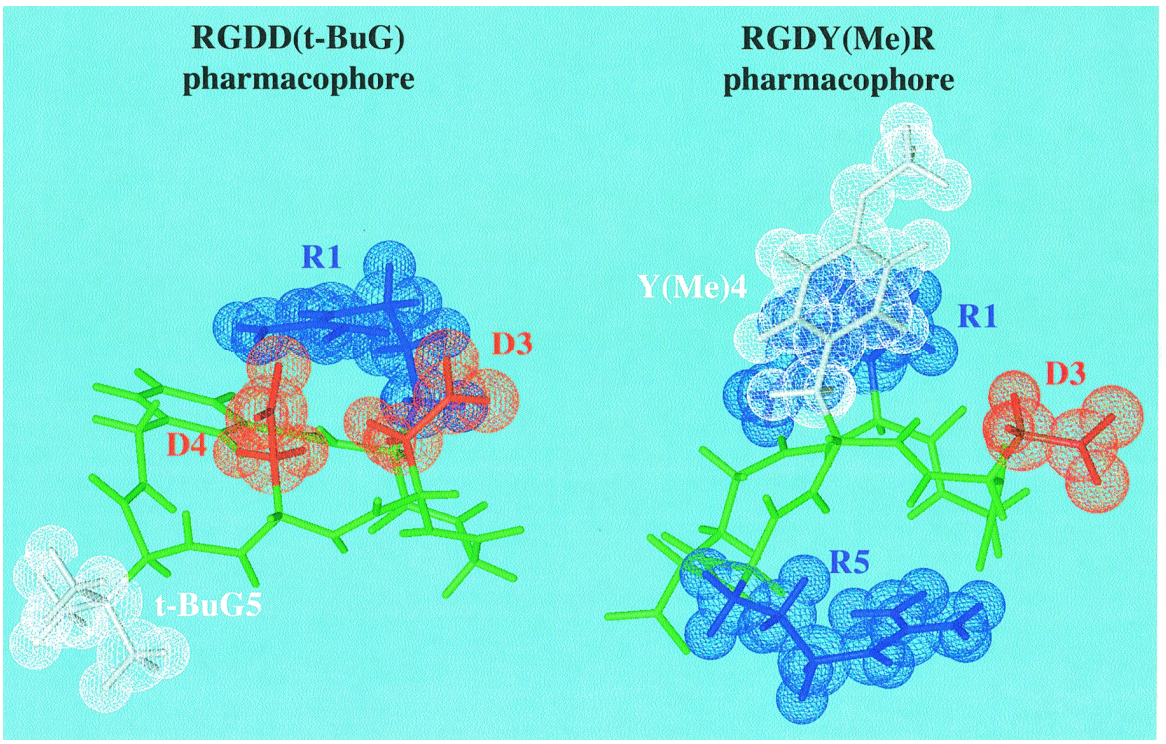

Plate 1 View of the RGDD(t-BuG) and RGDY(Me)R pharmacophore models. Negative and positive ionizable side chains are indicated by red and blue spheres respectively. Hydrophobic moieties are indicated in white.

plained by the greater flexibility shown by molecular modeling probably due to the disulfide cyclization.

Peptides which contain the 2,7-(aminomethyl)naphthoic acid (2,7-Amn) linker have weak or no affinity to the $\alpha_v\beta_3$ receptor (Table 1 entry 5, 6). The backbone structure of the RGD sequence determined in the proposed pharmacophore model of the RGDDV and the RGDY(Me)R sequences is maintained in these molecules. However, the β-turn in the RGD sequence is held in a conformation in which the Arg^1C^β-Asp^3C^β distance is too long for optimal binding to $\alpha_v\beta_3$ (> 7 Å).

In conclusion, by comparing conformational arrays found in solution of six cyclic peptides, four of which contain the RGDDV pharmacophore and two with the RGDY(Me)R sequence, structural elements in the pharmacophore models relevant for activity were discussed. Molecular modeling studies confirm the conformations chosen are consistent with the reported Arg^1C^β-Asp^3C^β distance necessary for binding to $\alpha_v\beta_3$. Of interest is the fact that of all the conformations observed in solution, only the discussed pharmacophore models have a distance of < 6 Å. Our studies show that this distance is modulated by the position of the β-turn in the RGD sequence, by the conformation of the *C*-terminal tripeptide sequence [DD(*t*-BuG) or DY(Me)R] of the pentapeptide pharmacophore, and by the linker used to cyclize and constrain the peptide.

Acknowledgements

This work was supported by a grant from the National Institute of Health (DK5 193 8) and a grant from Integra LifeSciences Corporation, Corporate Research Center. The authors would like to thank Tim Malaney, Bob Minasyan, and Gaylord Paulson of Integra LifeSciences Corporation for peptide synthesis and purification.

REFERENCES

1. Ruoslahti E, Pierschbacher MD. *Science* 1987; **238**: 491–497.
2. Seftor REB, Seftor EA, Gehlsen KR, Stetler-Stevenson WG, Brown PD, Ruoslahti E, Hendrix MJC. *Proc. Natl. Acad. Sci. USA* 1992; **89**: 1557–1561.
3. Drake CJ, Cheresh DA, Little CD. *J. Cell Sci.* 1995; **108**: 2655–2661.
4. Brooks PC, Stromblad S, Klemke R, Visscher D, Sarkar FH, Cheresh DA. *J. Clin. Invest.* 1995; **96**: 1815–1822.
5. Aumailley M, Gurrath M, Müller G, Calvete J, Timpl R, Kessler H. *FEBS Letters* 1991; **291**: 50–54.
6. Gurrath M, Müller G, Kessler H, Aumailley M, Timpl R. *Eur. J. Biochem.* 1992; **210**: 911–921.
7. Haubner R, Schmitt W, Hölzemann G, Goodman SL, Jonczyk A, Kessler H. *J. Am. Chem. Soc.* 1996; **118**: 7881–7891.
8. Haubner R, Gratias R, Diefenbach B, Goodman SL, Jonezyk A, Kessler H. *J. Am. Chem. Soc.* 1996; **118**: 7461–7472.
9. Burgess K, Lim D, Mousa SA. *J. Med. Chem.* 1996; **39**: 4520–4526.
10. Keenan RM, Miller WH, Kwon C, Ali FE, Callahan JF, Calvo RR, Hwang S-M, Kopple KD, Peishoff CE, Samanen JM, Wong AS, Yuan CK, Huffman WF. *J. Med. Chem.* 1997; **40**: 2289–2292.
11. Mullen DG, Cheng S, Ahmed S, Blevitt JM, Bonnin D, Craig WS, Ingram RT, Mazur C, Minasyan R, Tolley JO, Tschopp JF, Pierschbacher MD. Peptides: chemistry, structure and biology. *Proceedings of the 14th American Peptide Symposium*, Kaumaya PT, Hodges RS (eds). Mayflower Scientific Ltd: West Midlands, UK, 1995; 207–208.
12. Jennings LK, Phillips DR. *J. Biol. Chem.* 1982; **257**: 10458–10466.
13. Coller BS, Peerschke EI, Scudder LE, Sullivan CA. *J. Clin. Invest.* 1983; **72**: 325–338.
14. Shadle PJ, Ginsberg MH, Plow EF, Barondes SH. *J. Cell. Biol.* 1984; **99**: 2056–2060.
15. Tschopp JF, Driscoll EM, Mu D-X, Black SC, Pierschbacher MD, Lucchesi BR. *Coron. Artery Dis.* 1993; **4**: 809–817.
16. Cheng S, Craig WS, Mullen D, Tschopp JF, Dixon D, Pierschbacher MP. *J. Med. Chem.* 1994; **37**: 1–8.
17. Müller G, Gurrath M, Kessler H, Timpl R. *Angew. Chem. Int. Ed. Engl.* 1992; **31**: 326–328.
18. Bean JW, Kopple KD, Peishoff CE. *J. Am. Chem. Soc.* 1992; **114**: 5326–5334.
19. Peishoff CE, Ali FE, Bean JW, Calvo R, D'Ambrosio CA, Eggleston DS, Hwang SM, Kline TP, Koster PF, Nichols A, Powers D, Romoff T, Samanen JM, Stadel J, Vasko JA, Kopple KD. *J. Med. Chem.* 1992; **35**: 3962–3969.
20. Bogusky MJ, Naylor AM, Pitzenberger SM, Nutt RF Brady SF, Colton CD, Sisko JT, Anderson PS, Veber DF. *Int. J. Peptide Protein Res.* 1992; **39**: 63–76.
21. Bogusky MJ, Naylor AM, Mertzman ME, Pitzenberger SM, Nutt RF, Brady SF, Colton CD, Veber DF. *Biopolymers* 1993; **33**: 1287–1297.
22. Sanderson PN, Glen RC, Payne AWR, Hudson BD, Heide C, Tranter GE, Doyle PM, Harris C. J. *Int. J. Peptide Protein Res.* 1994; **43**: 588–596.
23. Mierke DF, Kurz M, Kessler H. *J. Am. Chem. Soc.* 1994; **116**: 1042–1049.
24. Davies JS, Enjalbal C, Wise CJ, Webb SE, Gareth EJ. *J. Chem. Soc. Perkin Trans.* 1994; **1**: 2011–2015.
25. Kessler H, Diefenbach B, Finsinger D, Geyer A, Gurrath M, Goodman SL, Hölzemann G, Haubner R,

Jonezyk A, Muller G, Graf von Roedern E, Wermuth J. *Lett. Pept. Sci.* 1995; **2**: 155–160.
26. Pfaff M, Tangemann K, Muller B, Gurrath M, Muller G, Kessler H, Timpl R, Engel J. *J. Biol. Chem.* 1994; **269**: 20233–20238.
27. Bach AC II, Espina JR, Jackson SA, Stouten PFW, Duke JL, Mousa SA, DeGrado WF. *J. Am. Chem. Soc.* 1996; **118**: 293–294.
28. Wüthrich K. *NMR of Proteins and Nucleic Acids*. Wiley: New York, 1986.
29. Aue WP, Bartholdi E, Ernst RR. *J. Chem. Phys.* 1976; **64**: 2229–2246.
30. Bax A, Freeman R. *J. Magn. Reson.* 1981; **44**: 542–561.
31. Rance M, Sorensen OW, Bodenhausen G, Wagner G, Ernst RR, Wüthrich K. *Biochem. Biophys. Res. Comm.* 1984; **117**: 479–485.
32. Kumar A, Ernst RR, Wüthrich K. *Biochem. Biophys. Res. Commun.* 1980; **95**: 1–6.
33. Davis D, Bax A. *J. Amer. Chem. Soc.* 1985; **107**: 2820–2821.
34. Bothner-By AA, Stephens RL, Lee J, Warren CD, Jeanloz RW. *J. Amer. Chem. Soc.* 1984; **106**: 811–813.
35. *Felix 95.0 User Guide*. Biosym/MSI: San Diego, CA, 1995.
36. Yamazaki T, Abe A. *Biopolymers* 1988; **27**: 969–984.
37. Pachler KGP. *Spectrochim. Acta* 1964; **20**: 581–587.
38. Cung MT, Marraud M. *Biopolymers* 1982; **21**: 953–967.
39. *NMRchitect User Guide*, *Version 2.3*. Biosym/MSI: San Diego, CA, 1993.
40. Bystrov VF, Ivanov VT, Portanova SL, Balashova TA, Ovchinnikov YA. *Tetrahedron* 1973; **29**: 873–877.
41. Cung MT, Marraud M, Neel J. *Macromolecules* 1974; **7**: 606–613.
42. *Discover 95.0/3.00 User Guide*. Biosym/MSI: San Diego, CA, 1995.

